

Nontopological first-order vortices in a gauged $CP(2)$ theory endowed with the Chern-Simons action

R. Casana¹, M. L. Dias¹ and E. da Hora².

¹*Departamento de Física, Universidade Federal do Maranhão,
65080-805, São Luís, Maranhão, Brazil.*

²*Coordenadoria Interdisciplinar de Ciência e Tecnologia,
Universidade Federal do Maranhão,
65080-805, São Luís, Maranhão, Brazil.*

We study a gauged $CP(2)$ model with the Chern-Simons term, focusing our attention on those time-independent radially symmetric configurations with nontopological profile. We proceed the minimization of the effective energy in order to introduce the corresponding first-order framework, from which we define a legitimate self-dual scenario. We solve the resulting first-order equations numerically by means of the finite-difference scheme, from which we depict the nontopological solutions. We also identify a special kind of solutions which can be partially described by an analytical treatment.

PACS numbers: 11.10.Kk, 11.10.Lm, 11.27.+d

I. INTRODUCTION

In the context of classical field models, vortices are those time-independent radially symmetric solutions arising from a planar gauged theory in the presence of a symmetry breaking potential describing the scalar-matter self-interaction [1]. However, due to the high nonlinearity inherent to the symmetry breaking potentials, the corresponding Euler-Lagrange equations of motion can be quite hard to solve (even numerically).

On the other hand, under very special circumstances, time-independent vortices can also be obtained by solving a particular set of coupled first-order differential equations (instead of the second-order Euler-Lagrange ones), these equations being usually obtained via the minimization of the effective energy, the resulting solutions saturating a well-defined lower bound for the energy itself [2].

In this sense, first-order vortices were firstly obtained in the context of the Maxwell-Higgs electrodynamics in which the corresponding vacuum manifold exhibits asymmetric states only (the resulting vortices presenting the typical topological behavior) [3]. In addition, first-order vortices were verified to occur also in the Chern-Simons-Higgs theory, with the vacuum structure presenting now both symmetric and asymmetric states (the corresponding configurations being topological or nontopological, respectively) [4].

Furthermore, legitimate vortex solutions satisfying first-order differential equations were also investigated in connection to the noncanonical gauge theories [5], the resulting structures being applied in the study of some interesting cosmological problems [6].

In such a context, an interesting issue is the search for the first-order vortices inherent to a gauged $CP(N-1)$ model, mainly due to the phenomenological connection between such a theory and the four-dimensional Yang-Mills-Higgs one [7].

In this sense, in a recent work, the time-independent

solutions with radial symmetry arising from a gauged $CP(2)$ model in the presence of the Maxwell's term were studied, the author focusing his attention on how some relevant quantities (such as the total energy and the magnetic field) depend on the parameters defining the model [8]. In that work, however, these configurations were obtained directly from the second-order Euler-Lagrange equations of motion.

In the sequel, some of us have developed a particular first-order framework consistent with the very same theoretical scenario described above. Indeed, we have proceeded the minimization of the resulting energy, from which we have introduced the corresponding first-order equations and a well-defined lower bound for the energy itself, the potential supporting self-duality presenting only asymmetric vacua, which we have used to study time-independent vortices with a topological profile [9].

We have also studied the radially symmetric solitons inherent to a planar $CP(2)$ model endowed by the Maxwell's term multiplied by a nontrivial dielectric function, our main conclusion being that the potential (and the vacuum manifold it defines) supporting self-duality depends on the dielectric function itself [10]. We have then chosen such a function in order to change the original vacuum manifold into a dot surrounded by a circle (the centered dot representing a symmetric vacuum), from which we have obtained nontopological vortices with no electric charge.

Furthermore, we have recently considered a $CP(2)$ theory in the presence of the Chern-Simons term (instead of the Maxwell's one), via which we have verified the existence of first-order vortices with a nonvanishing electric field, the resulting configurations presenting the well-known topological profile [11].

Now, we go a little bit further on the aforementioned investigation by studying those nontopological vortices satisfying the first-order framework consistent with the gauged $CP(2)$ model endowed by the Chern-Simons action.

In order to present our results, this work is organized

as follows: in the next Section II, we introduce the overall model and the conventions inherent to it, focusing our attention on those radially symmetric time-independent configurations. We then proceed the minimization of the effective energy, from which we introduce the corresponding first-order framework (i.e. the first-order equations themselves and a well-defined lower bound for the total energy). In the Section III, we use those expressions in order to define a coherent first-order scenario, the starting-point being a differential constraint whose solution is the particular potential supporting self-duality. We write down the resulting first-order equations and the boundary conditions engendering finite-energy configurations with no divergences. We solve the first-order equations numerically by means of the finite-difference scheme, from which we depict the solutions to the relevant fields. We implement a convenient assumption, from which we get an approximate analytical description of those numerical solutions, therefore explaining in details their main properties. We also identify a second type of numerical solutions that can not be predicted by any analytical treatment. Finally, in the last Section IV, we present our main conclusions and perspectives regarding future investigations.

In what follows, we use $\eta^{\mu\nu} = (+ - -)$ as the metric signature for the flat spacetime, together with the natural units system, for the sake of convenience.

II. THE MODEL

We begin our letter by reviewing the first-order formalism presented in [11], the starting-point being the planar Lagrange density describing the interaction between the electromagnetic field (introduced via the Chern-Simons term) and the complex $CP(N-1)$ one, i.e. (here, $\epsilon^{012} = +1$)

$$L = -\frac{k}{4}\epsilon^{\alpha\mu\nu}A_\alpha F_{\mu\nu} + (P_{ab}D_\mu\phi_b)^* P_{ac}D^\mu\phi_c - V(|\phi|), \quad (1)$$

the $CP(N-1)$ sector itself being constrained to satisfy $\phi_a^*\phi_a = h$. Here,

$$F_{\mu\nu} = \partial_\mu A_\nu - \partial_\nu A_\mu \quad (2)$$

is the electromagnetic field strength tensor and

$$D_\mu\phi_a = \partial_\mu\phi_a - igA_\mu Q_{ab}\phi_b \quad (3)$$

stands for the usual covariant derivative (in which Q_{ab} is a diagonal real matrix). Also, $P_{ab} = \delta_{ab} - h^{-1}\phi_a\phi_b^*$ is a projection operator.

The Euler-Lagrange equation for the electromagnetic field coming from (1) is

$$\frac{k}{2}\epsilon^{\lambda\mu\nu}F_{\mu\nu} = J^\lambda, \quad (4)$$

where

$$J^\lambda = ig \left(P_{ac}D^\lambda\phi_c (P_{ab}Q_{bf}\phi_f)^* - (P_{ab}D^\lambda\phi_b)^* P_{ac}Q_{cb}\phi_b \right) \quad (5)$$

is the current 4-vector. The Gauss law for time-independent configurations therefore reads

$$kB = \rho, \quad (6)$$

where $B = F_{21}$ stands for the magnetic field and

$$\rho = ig \left((P_{ab}D^0\phi_b)^* P_{ac}Q_{cd}\phi_d - P_{ab}D^0\phi_b (P_{ac}Q_{cd}\phi_d)^* \right) \quad (7)$$

represents the charge density. Here, given that $A^0 = 0$ does not solve (6) identically, we conclude that the time-independent structures arising from (1) are electrically charged.

In what follows, we focus our attention on those time-independent radially symmetric solutions defined by the usual vortex map

$$A_i = -\frac{1}{gr}\epsilon^{ij}n^j A(r), \quad (8)$$

$$\begin{pmatrix} \phi_1 \\ \phi_2 \\ \phi_3 \end{pmatrix} = h^{\frac{1}{2}} \begin{pmatrix} e^{im_1\theta} \sin(\alpha(r)) \cos(\beta(r)) \\ e^{im_2\theta} \sin(\alpha(r)) \sin(\beta(r)) \\ e^{im_3\theta} \cos(\alpha(r)) \end{pmatrix}, \quad (9)$$

where m_1, m_2 and m_3 are positive integers defining the vorticity of the resulting configurations. Also, ϵ^{ij} is the planar Levi-Civita symbol ($\epsilon^{12} = +1$) and $n^j = (\cos\theta, \sin\theta)$ stands for the unit vector.

Here, we point out that regular solutions presenting no divergences are attained via those profile functions $\alpha(r)$ and $A(r)$ satisfying the conditions

$$\alpha(r \rightarrow 0) \rightarrow 0 \quad \text{and} \quad A(r \rightarrow 0) \rightarrow 0, \quad (10)$$

which will be used later below.

Now, it is important to highlight that, regarding the combination between the winding numbers m_1, m_2 and m_3 and the charge matrix Q_{ab} , there are two different choices supporting the existence of topologically nontrivial configurations (both ones with $m_3 = 0$): (i) $m_1 = -m_2 = m$ and $Q = \lambda_3/2$ (with $\lambda_3 = \text{diag}(1, -1, 0)$), and (ii) $m_1 = m_2 = m$ and $Q = \lambda_8/2$ ($\sqrt{3}\lambda_8 = \text{diag}(1, 1, -2)$). However, it is known that these two scenarios simply mimic each other, being then phenomenologically equivalent. Therefore, in this manuscript, we consider only the first choice, i.e.

$$Q = \frac{1}{2}\text{diag}(1, -1, 0), \quad (11)$$

with $m_1 = -m_2 = m$ and $m_3 = 0$.

In this case, the radially symmetric Euler-Lagrange equation for the additional profile function $\beta(r)$ reads

$$\frac{d^2\beta}{dr^2} + \left(\frac{1}{r} + 2 \cot\alpha \frac{d\alpha}{dr} \right) \frac{d\beta}{dr} = H \sin^2\alpha \sin(4\beta), \quad (12)$$

where

$$H(r) = \frac{1}{r^2} \left(m - \frac{A}{2} \right)^2 - \frac{g^2 (A_0)^2}{4} \sin^2 \alpha \quad (13)$$

is an auxiliary function, the solutions for $\beta(r)$ being ($k \in \mathbb{Z}$)

$$\beta(r) = \beta_1 = \frac{\pi}{4} + \frac{\pi}{2}k \quad \text{or} \quad \beta(r) = \beta_2 = \frac{\pi}{2}k, \quad (14)$$

this way defining two a priori different scenarios.

Here, it is important to emphasize that the developments we introduce from now on effectively describe the particular scenarios defined by the choices we have specified in the previous paragraphs, the solutions for $\beta(r)$ being necessarily one of those in (14).

We look for the first-order differential equations by proceeding the minimization of the energy according the Bogomol'nyi prescription, the starting-point being the energy-momentum tensor itself, i.e.

$$T_{\lambda\rho} = 2 (P_{ab} D_\lambda \phi_b)^* P_{ac} D_\rho \phi_c - \eta_{\lambda\rho} L_{ntop}, \quad (15)$$

where

$$L_{ntop} = (P_{ab} D_\mu \phi_b)^* P_{ac} D^\mu \phi_c - V(|\phi|) \quad (16)$$

stands for the nontopological sector of the original Lagrange density (1).

The radially symmetric expression for the energy-density coming from (15) reads

$$\varepsilon(r) = \frac{k^2 B^2}{g^2 h W} + h \left[\left(\frac{d\alpha}{dr} \right)^2 + \frac{W}{r^2} \left(\frac{A}{2} - m \right)^2 \right] + V, \quad (17)$$

where we have used the radially symmetric Gauss law

$$A^0 = -\frac{2kB}{g^2 h W}, \quad (18)$$

with

$$W(\alpha, \beta) = (1 - \sin^2 \alpha \cos^2(2\beta)) \sin^2 \alpha \quad (19)$$

standing for an auxiliary function introduced conveniently.

We then suppose that the functions $W(\alpha, \beta)$ and $V(\alpha)$ are constrained to each other via

$$\frac{2k}{\sqrt{h}} \frac{d}{dr} \sqrt{\frac{V}{W}} = -g^2 h \sqrt{W} \frac{d\alpha}{dr}, \quad (20)$$

from which one gets that the total energy arising from (17) can be written as (here, $B(r) = -A'/gr$ is the radially symmetric magnetic field, with the prime denoting derivative with respect to the radial coordinate r)

$$\begin{aligned} \frac{E}{2\pi} &= h \int \left(\frac{d\alpha}{dr} \mp \frac{\sqrt{W}}{r} \left(\frac{A}{2} - m \right) \right)^2 r dr \\ &+ \int \left(\frac{kB}{g\sqrt{hW}} \mp \sqrt{V} \right)^2 r dr \\ &+ \int r \varepsilon_{bps} dr \geq \frac{E_{bps}}{2\pi}, \end{aligned} \quad (21)$$

with

$$E_{bps} = 2\pi \int r \varepsilon_{bps} dr \quad (22)$$

and

$$\varepsilon_{bps} = \mp \frac{2k}{g^2 \sqrt{h}} \frac{1}{r} \frac{d}{dr} \left[(A - 2m) \sqrt{\frac{V}{W}} \right]. \quad (23)$$

In this sense, the resulting first-order equations are

$$\frac{d\alpha}{dr} = \pm \frac{\sqrt{W}}{r} \left(\frac{A}{2} - m \right), \quad (24)$$

$$kB = \pm g \sqrt{h V W}, \quad (25)$$

from which we summarize the scenario as follows: given the potential $V(\alpha)$ satisfying the constraint (20) and the profile functions $\alpha(r)$ and $A(r)$ solving the differential equations (24) and (25), the radially symmetric configurations that the model (1) supports saturate the lowest energy possible (the Bogomol'nyi bound), i.e.

$$E = E_{bps} = \mp \frac{4\pi k}{g^2 \sqrt{h}} \left[(A_\infty - 2m) \sqrt{\frac{V_\infty}{W_\infty}} + 2m \sqrt{\frac{V_0}{W_0}} \right], \quad (26)$$

the upper (lower) sign holding for negative (positive) values of m . Here, we have defined $A_\infty \equiv A(r \rightarrow \infty)$, $V_\infty \equiv V(r \rightarrow \infty)$, $V_0 \equiv V(r \rightarrow 0)$ and so on, both $(A_\infty - 2m) \sqrt{V_\infty/W_\infty}$ and $\sqrt{V_0/W_0}$ being finite and positive.

In addition, it is worthwhile to point out that the asymptotic contribution appearing in the energy bound (26) stands for an essential difference in comparison to the topological case, in which such a contribution does not occur, the corresponding bound coming exclusively from the fields calculated near the origin, as the reader can verify via the Eq. (18) of the Ref. [11].

It is instructive to clarify that the energy of the first-order vortices inherent to a gauged scenario is expected to be proportional to the magnetic flux Φ_B that they engender. In this sense, we calculate the flux Φ_B as

$$\Phi_B = 2\pi \int r B(r) dr = -\frac{2\pi}{g} A_\infty. \quad (27)$$

We demonstrate below that the energy-bound (26) is indeed proportional to the magnetic flux (27), both quantities being not necessarily quantized, as expected for nontopological solitons.

III. FIRST-ORDER SOLUTIONS

We now use the first-order expressions that we have introduced to obtain legitimate nontopological configurations. In this sense, we proceed as follows: firstly,

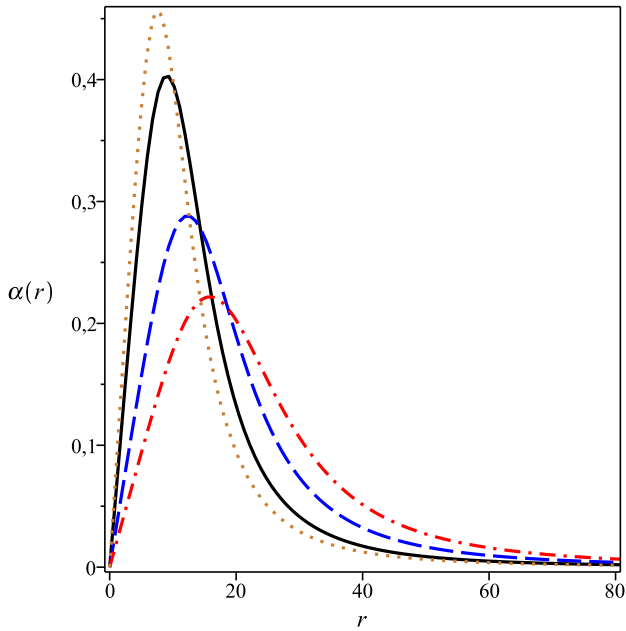


FIG. 1: Numerical solutions to $\alpha(r)$ coming from the first-order equations (33) and (34) in the presence of the boundary conditions (10) and (32). Here, we have chosen $m = h = g = k = 1$ and $r_0 = 10$ (solid black line), $r_0 = 15$ (dashed blue line) and $r_0 = 20$ (dash-dotted red line). We have also plotted the approximate analytical solution (44) for $m = h = g = k = 1$ and $r_0 = 10$ (dotted orange line), for comparison.

we choose a particular solution for $\beta(r)$ between those in (14), from which we solve the differential constraint (20) for the potential $V(\alpha)$ supporting self-duality. We then implement these results in the radially symmetric energy density (17), this way finding the asymptotic conditions that the profile functions $\alpha(r)$ and $A(r)$ must obey in order to fulfill the finite-energy requirement $\varepsilon(r \rightarrow \infty) \rightarrow 0$. In the sequel, we write down the corresponding first-order equations, solving them numerically by means of the finite-difference scheme, from which depict the resulting profiles and comment on the main properties that they engender.

However, concerning the first-order solutions inherent to (1), the two a priori different scenarios defined by (14) can be verified to map each other via the redefinitions $\alpha \rightarrow 2\alpha$ and $h \rightarrow h/4$, the results for $\beta(r) = \beta_2$ being then obtained directly from those for $\beta(r) = \beta_1$, therefore existing only one effective scenario. In this sense, in what follows, we consider the case $\beta(r) = \beta_1$ only.

In this sense, we choose

$$\beta(r) = \frac{\pi}{4} + \frac{\pi}{2}k, \quad (28)$$

from which one gets $\cos^2(2\beta_1) = 0$ and $W(\alpha, \beta_1) = \sin^2 \alpha$, the constraint (20) reducing to

$$\frac{2k}{g^2\sqrt{h}} \frac{d}{dr} \left(\frac{\sqrt{V}}{\sin \alpha} \right) = h \frac{d}{dr} (\cos \alpha), \quad (29)$$

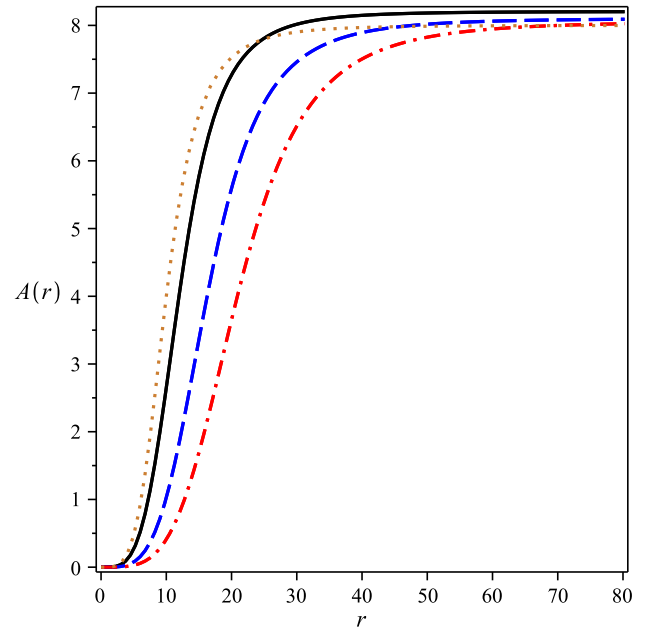


FIG. 2: Numerical solutions to $A(r)$. Conventions as in the Fig. 1. The solutions approach $A_m(r \rightarrow \infty) = 4(m+1)$, the numerical values being $A_1(r \rightarrow \infty) \approx 8.20526$ for $r_0 = 10$, $A_1(r \rightarrow \infty) \approx 8.10268$ for $r_0 = 15$ and $A_1(r \rightarrow \infty) \approx 8.06025$ for $r_0 = 20$.

whose solution is

$$V(\alpha) = \frac{g^4 h^3}{16k^2} \sin^2(2\alpha), \quad (30)$$

which stands for the self-dual potential. Here, we have used $C = 0$ for the integration constant.

Now, in view of (28) and (30), the energy density (17) can be rewritten in the form

$$\varepsilon(r) = \frac{k^2 B^2}{g^2 h \sin^2 \alpha} + \frac{g^4 h^3}{16k^2} \sin^2(2\alpha) + h \left[\left(\frac{d\alpha}{dr} \right)^2 + \frac{\sin^2 \alpha}{r^2} \left(\frac{A}{2} - m \right)^2 \right], \quad (31)$$

from which we attain $\varepsilon(r \rightarrow \infty) \rightarrow 0$ (the finite-energy requirement) by imposing (prime denoting derivative with respect to r)

$$\alpha(r \rightarrow \infty) \rightarrow 0 \quad \text{and} \quad A'(r \rightarrow \infty) \rightarrow 0, \quad (32)$$

with $A_\infty \equiv A(r \rightarrow \infty)$ to be determined below. In the present case, the first-order equations (24) and (25) then read

$$\frac{d\alpha}{dr} = \pm \frac{\sin \alpha}{r} \left(\frac{A}{2} - m \right), \quad (33)$$

$$\frac{1}{r} \frac{dA}{dr} = \mp \frac{g^4 h^2}{4k^2} \sin(2\alpha) \sin \alpha, \quad (34)$$

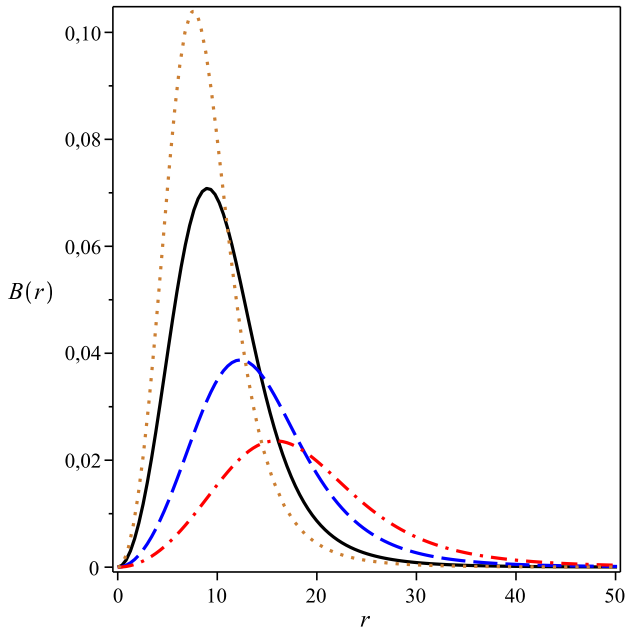


FIG. 3: Numerical solutions to the magnetic field $B(r)$. Conventions as in the Fig. 1. The resulting configurations are rings centered at the origin, their radii being given by (43). In particular, $B_m(r = r_{\max}) \propto r_0^{-2}$, decreasing as r_0 increases.

the upper (lower) sign holding for negative (positive) values of m .

Here, it is interesting to point out that, due to the conditions $\alpha(r \rightarrow 0) \rightarrow 0$ and $\alpha(r \rightarrow \infty) \rightarrow 0$, the first-order equations (33) and (34) can be verified to support approximate analytical solutions. In order to calculate them, we suppose that $\alpha(r) \ll 1$ for all r , from which those equations can be approximated, respectively, by

$$\frac{d\alpha}{dr} = \pm \frac{\alpha}{r} \left(\frac{A}{2} - m \right), \quad (35)$$

$$\frac{1}{r} \frac{dA}{dr} = \mp \frac{g^4}{2k^2} h^2 \alpha^2, \quad (36)$$

therefore giving rise to Liouville's equation (here, $\lambda^2 = g^4 h^2 / k^2$)

$$\frac{d^2}{dr^2} \ln \alpha^2 + \frac{1}{r} \frac{d}{dr} \ln \alpha^2 + \frac{\lambda^2}{2} \alpha^2 = 0, \quad (37)$$

its solution standing for

$$\alpha(r) = \frac{4C_1}{\lambda r_0} \frac{\left(\frac{r}{r_0}\right)^{C_1-1}}{1 + \left(\frac{r}{r_0}\right)^{2C_1}}, \quad (38)$$

where r_0 and C_1 are integration constants. Here, it is worthwhile to highlight that, in order to fulfill the asymptotic condition $\alpha(r \rightarrow \infty) \rightarrow 0$, we must choose $C_1 > 1$.

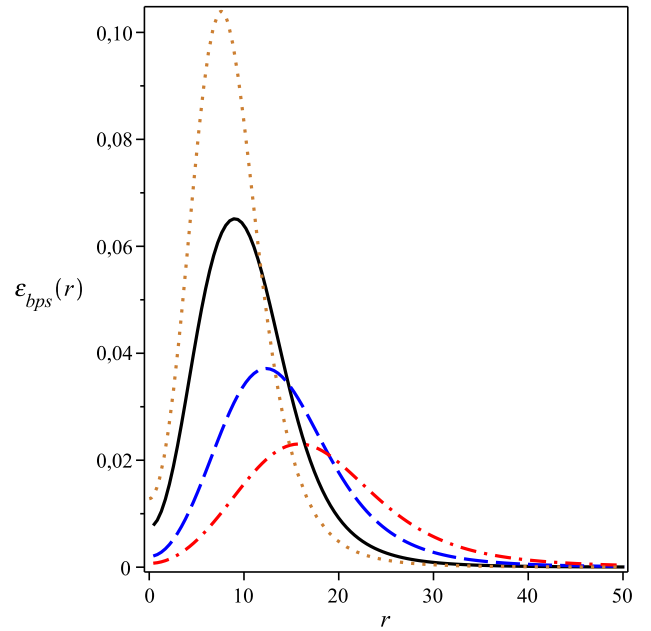


FIG. 4: Numerical solutions to the energy density $\varepsilon_{bps}(r)$. Conventions as in the Fig. 1. Here, $\varepsilon_{bps,m}(r=0) \propto r_0^{-4}$ for $m = 1$ and $\varepsilon_{bps,m}(r=0) = 0$ for $m > 1$.

In addition, given (35) and (38), one gets that the solution to $A(r)$ reads

$$A(r) = 2(m+1 - C_1) + \frac{4C_1 \left(\frac{r}{r_0}\right)^{2C_1}}{1 + \left(\frac{r}{r_0}\right)^{2C_1}}, \quad (39)$$

which satisfies the condition $A(r \rightarrow 0) \rightarrow 0$ for $C_1 = m + 1$ only.

The approximate solutions can then be summarized as

$$\alpha_m(r) = \frac{4(m+1)}{\lambda r_0} \frac{\left(\frac{r}{r_0}\right)^m}{1 + \left(\frac{r}{r_0}\right)^{2(m+1)}}, \quad (40)$$

$$A_m(r) = 4(m+1) \frac{\left(\frac{r}{r_0}\right)^{2(m+1)}}{1 + \left(\frac{r}{r_0}\right)^{2(m+1)}}, \quad (41)$$

the last one giving rise to

$$A_{m,\infty} \equiv A_m(r \rightarrow \infty) = 4(m+1), \quad (42)$$

standing for the (approximate) asymptotic condition to be imposed on $A(r)$.

It is interesting to note that the approximate solution to $\alpha_m(r)$ stands for a well-defined ring, its radius being given by

$$r_{\max} = r_0 \left(\frac{m}{m+2} \right)^{\frac{1}{2(m+1)}}, \quad (43)$$

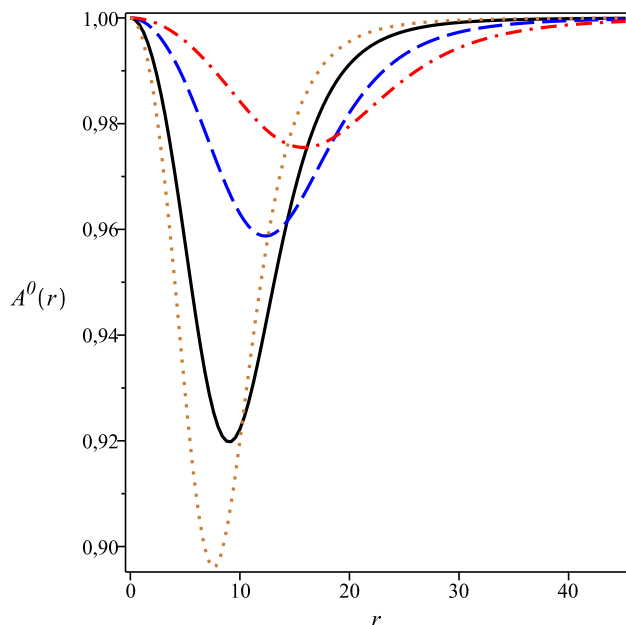


FIG. 5: Numerical solutions to the electric potential $A^0(r)$. Conventions as in the Fig. 1. Here, $A_m^0(r=0) = A_m^0(r \rightarrow \infty) = gh/k$, with $A_m^0(r=r_{\max})$ vanishing for $r_0 \rightarrow \infty$.

(r_{\max} approaching r_0 in the limit $m \rightarrow \infty$), from which one gets

$$\alpha_m(r=r_{\max}) = \frac{2(m+2)}{\lambda r_0} \left(\frac{m}{m+2} \right)^{\frac{m}{2(m+1)}}, \quad (44)$$

i.e. the amplitude of the ring, our previous assumption $\alpha(r) \ll 1$ holding for

$$\lambda r_0 \gg 2(m+2) \left(\frac{m}{m+2} \right)^{\frac{m}{2(m+1)}}, \quad (45)$$

i.e., for a fixed m , there are only a few values to be chosen for λ and r_0 , and vice-versa.

In this sense, we solve the first-order equations (33) and (34) numerically for $m = h = g = k = 1$ and $r_0 = 10$ (solid black line), $r_0 = 15$ (dashed blue line) and $r_0 = 20$ (dash-dotted red line), from which we plot the resulting profiles in the figs. 1, 2, 3, 4, 5 and 6 below. We also depict the approximate solutions for $m = h = g = k = 1$ and $r_0 = 10$ (dotted orange line), for comparison.

The solutions to the profile function $\alpha(r)$ appear in the Figure 1. These profiles are well-defined rings centered at the origin, their radii and amplitudes being given, respectively, by (43) and (44), the first (second) one increasing (decreasing) as r_0 itself increases.

The Figure 2 shows the numerical results to the profile function $A(r)$. Here, it is interesting to note the way the solutions reach the approximate condition $A_m(r \rightarrow \infty) = 4(m+1)$, the numerical values reading $A_1(r \rightarrow \infty) \approx 8.20526$ for $r_0 = 10$, $A_1(r \rightarrow \infty) \approx 8.10268$ for $r_0 = 15$ and $A_1(r \rightarrow \infty) \approx 8.06025$ for

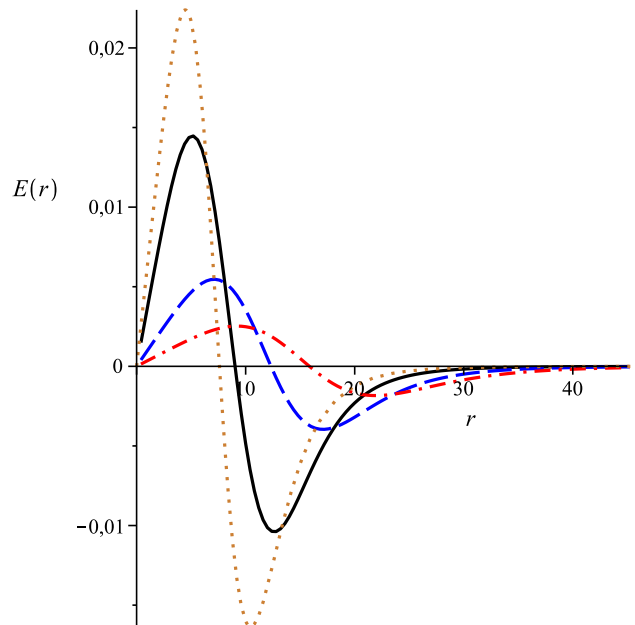


FIG. 6: Numerical solutions to the electric field $E(r)$. Conventions as in the Fig. 1. In this case, $r_{m=1,-} \approx 4.46485$ and $r_{m=1,+} \approx 10.46277$, with $E_{m=1}(r=r_{m=1,-}) \approx 0.02239$ and $E_{m=1}(r=r_{m=1,+}) \approx -0.01636$. Note the inversion of the sign dictating the electric interaction.

$r_0 = 20$, the overall solutions being monotonic, as expected.

In the Figure 3, we depict the profiles to the magnetic field $B(r)$, the resulting structures also standing for defined rings centered at $r = 0$ (here, both $B(r=0)$ and $B(r \rightarrow \infty)$ vanish). In particular, the approximate analytical solution to $B_m(r)$ arising from (40) and (41) reads

$$B_m(r) = \pm \frac{g^3 h^2}{2k^2} \alpha_m^2, \quad (46)$$

via which one concludes that the radii of the corresponding rings are also given by (43), the amplitudes being

$$B_m(r=r_{\max}) = \pm \frac{2g^3 h^2 (m+2)^2}{(\lambda r_0)^2 k^2} \left(\frac{m}{m+2} \right)^{\frac{m}{m+1}}, \quad (47)$$

which decrease as r_0 itself increases.

The numerical solutions to the energy density $\varepsilon_{bps}(r)$ are plotted in the Figure 4. In this case, it is worthwhile to point out that all the solutions fulfill the finite-energy requirement, i.e. $\varepsilon_{bps}(r \rightarrow \infty) \rightarrow 0$, the approximate expression for the energy distribution being

$$\varepsilon_{bps,m}(r) = \frac{g^4 h^3}{2k^2} \alpha_m^2 + 2h \frac{\alpha_m^2}{r^2} \left(\frac{A_m}{2} - m \right)^2, \quad (48)$$

which can be rewritten in the form (here, we have implemented the first-order equation (35))

$$\varepsilon_{bps,m}(r) = \frac{g^4 h^3}{2k^2} \alpha_m^2 + 2h \left(\frac{d\alpha_m}{dr} \right)^2, \quad (49)$$

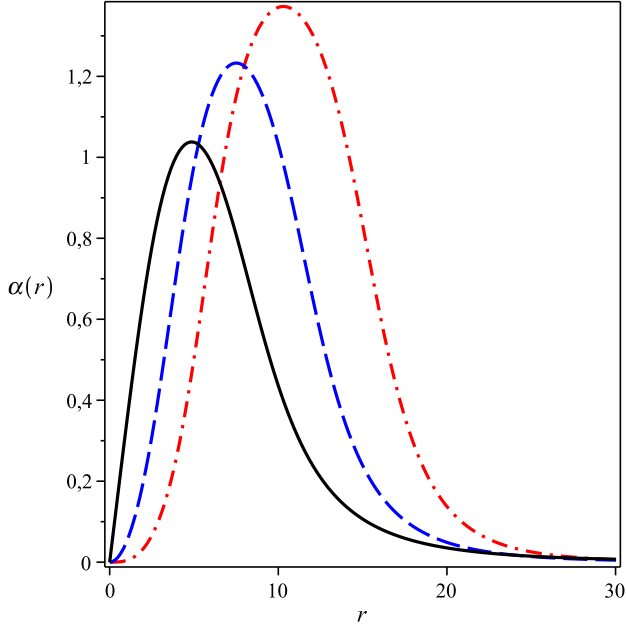


FIG. 7: Numerical solutions to $\alpha(r)$. Here, we have used $h = g = k = r_0 = 1$ and $m = 1$ (solid black line), $m = 2$ (dashed blue line) and $m = 3$ (dash-dotted red line), the resulting scenario being not predictable by any analytical treatment.

from which we get that the radii inherent to the energy-rings are also defined by the expression in (43). Moreover, we calculate

$$\varepsilon_{bps,m}(r = r_{\max}) = \frac{2h(m+2)^2}{r_0^2} \left(\frac{m}{m+2}\right)^{\frac{m}{m+1}} \quad (50)$$

and

$$\varepsilon_{bps,m}(r = 0) = \begin{cases} \frac{128m^2k^2}{g^4hr_0^4}, & \text{if } m = 1 \\ 0, & \text{if } m > 1 \end{cases}, \quad (51)$$

with $\varepsilon_{bps,1}(r = 0)$ decreasing as r_0 increases, see the numerical solutions.

We plot the numerical results to the electric potential $A^0(r)$ in the Figure 5, the approximate solution standing for

$$A_m^0(r) = \pm \frac{gh}{k} \left(1 - \frac{1}{2}\alpha_m^2\right), \quad (52)$$

the resulting profile satisfying $A_m^0(r = 0) = A_m^0(r \rightarrow \infty) = \pm gh/k$, these boundary conditions do not depending on m . Moreover, given (52), one concludes that the corresponding radius is also given by (44), via which we calculate

$$A_m^0(r = r_{\max}) = \pm \frac{gh}{k} \left(1 - \frac{2(m+2)^2}{(\lambda r_0)^2} \left(\frac{m}{m+2}\right)^{\frac{m}{m+1}}\right), \quad (53)$$

which vanishes in the limit $r_0 \rightarrow \infty$. In particular, for $m = h = g = k = 1$ and $r_0 = 10$, one gets that $A_{m=1}^0(r = r_{\max}) \approx 0.89608$, see the Figure 5.

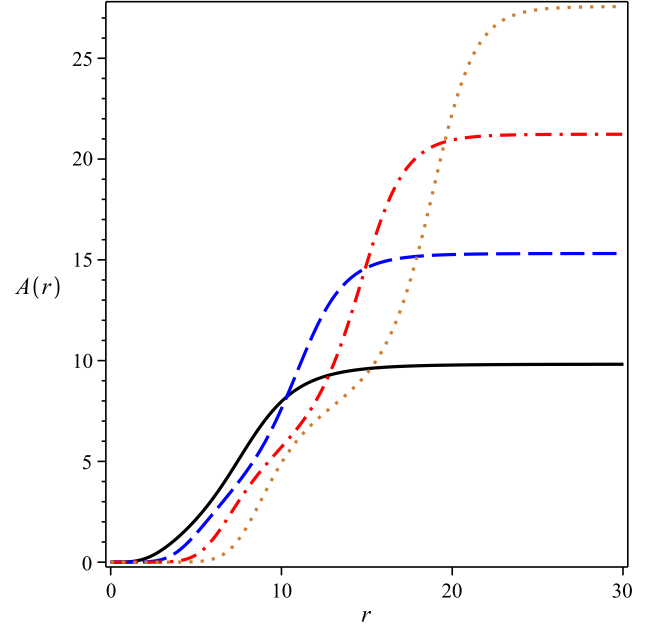


FIG. 8: Numerical solutions to $A(r)$. Conventions as in the Fig. 7, the dotted orange line representing the solution for $m = 4$, the resulting gauge profile presenting an internal structure.

The numerical solutions to the electric field $E(r) = -dA^0/dr$ appear in the Figure 6, the approximate one reading

$$E_m(r) = \frac{gh}{k} \frac{\alpha_m^2}{r} \left(\frac{A_m}{2} - m\right), \quad (54)$$

with $A_m(r)$ itself given by (41). In this case, one gets that

$$\frac{dE_m}{dr} = -\frac{d^2A_m^0}{dr^2} = \pm \frac{gh}{k} \left[\left(\frac{d\alpha_m}{dr}\right)^2 + \alpha_m \frac{d^2\alpha_m}{dr^2} \right] \quad (55)$$

vanishes for

$$\left(\frac{d\alpha_m}{dr}\right)^2 = -\alpha_m \frac{d^2\alpha_m}{dr^2}, \quad (56)$$

whose solutions are

$$r_{m,\mp} = r_0 R_{m,\mp}^{\frac{1}{2(m+1)}}, \quad (57)$$

in which

$$R_{m,\mp} = \frac{a_m \mp b_m}{c_m}, \quad (58)$$

the positive coefficients

$$a_m = 4m^2 + 8m + 1, \quad (59)$$

$$b_m = \sqrt{12m^4 + 48m^3 + 61m^2 + 26m + 1}, \quad (60)$$

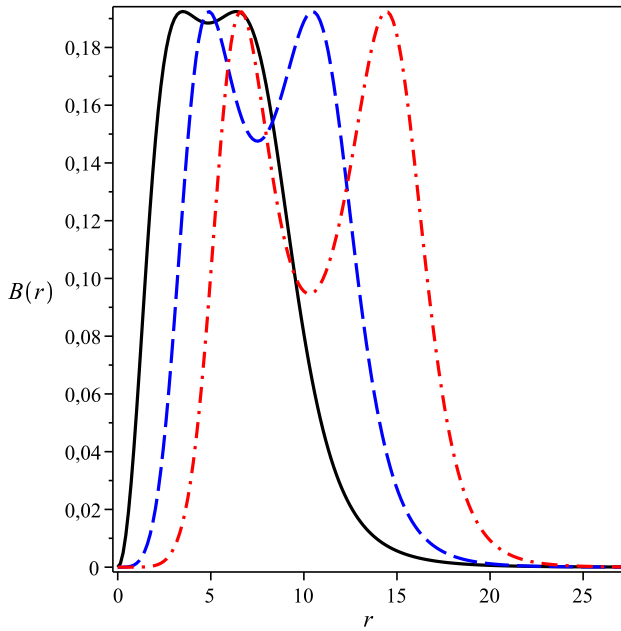


FIG. 9: Numerical solutions to $B(r)$. Conventions as in the Fig. 7. The solution is a double ring centered at the origin, the magnetic field vanishing at the boundaries.

and

$$c_m = 2m^2 + 9m + 10 \quad (61)$$

depending on the vorticity m explicitly.

In the Figure 6, $r_{m,-}$ and $r_{m,+}$ are the points in which the approximate solution (54) for the electric field reaches its extreme values, i.e.

$$E_m(r = r_{m,\mp}) = \frac{16(m+1)^2 gh}{\lambda^2 k r_0} \Sigma_{m,\mp} \quad (62)$$

for $m > 0$, and

$$E_m(r = r_{m,\mp}) = -\frac{16(m+1)^2 gh}{\lambda^2 k r_0} \Sigma_{m,\mp} \quad (63)$$

for $m < 0$, where

$$\Sigma_{m,\mp} = \frac{R_{\mp}^{\frac{2m-1}{2(m+1)}}}{(1 + R_{\mp})^3} (m - (m+2) R_{\mp}), \quad (64)$$

with both $E_m(r=0)$ and $E_m(r \rightarrow \infty)$ vanishing. In particular, again for $m = h = g = k = 1$ and $r_0 = 10$, we get that $r_{m=1,-} \approx 4.46485$ and $r_{m=1,+} \approx 10.46277$, with $E_{m=1}(r = r_{m=1,-}) \approx 0.02239$ and $E_{m=1}(r = r_{m=1,+}) \approx -0.01636$. Here, it is interesting to note the inversion in the sign dictating the electric interaction.

It is instructive to highlight that, in view of the analytical results we have obtained, the energy-bound (26) can be calculated explicitly, its approximate value being given by

$$\bar{E}_{bps} = \mp 8\pi h (m+1), \quad (65)$$

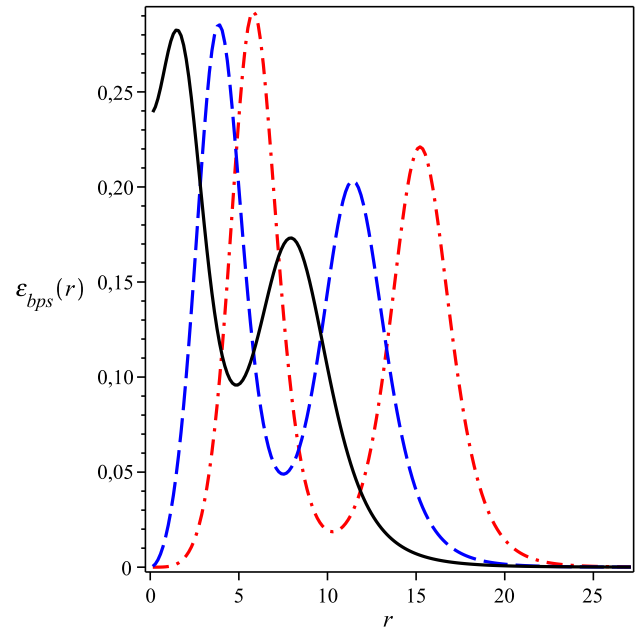


FIG. 10: Numerical solutions to $\varepsilon_{bps}(r)$. Conventions as in the Fig. 7, the energy distribution vanishing at $r = 0$ for $m \neq 1$ only.

the magnetic flux (27) standing for

$$\Phi_B = -\frac{8\pi}{g} (m+1), \quad (66)$$

from which one gets $E_{bps} = \pm gh\Phi_B$, the energy of the analytical first-order vortices being then proportional to their magnetic flux, as expected. Here, we have used

$$(A_\infty - 2m) \sqrt{\frac{V_\infty}{W_\infty}} = \frac{g^2 h^{\frac{3}{2}}}{k} (m+2) \quad (67)$$

and

$$\sqrt{\frac{V_0}{W_0}} = \frac{g^2 h^{\frac{3}{2}}}{2k}, \quad (68)$$

therefore verifying our previous assumption, see the discussion after (26).

However, we point out that both the energy and the magnetic flux of those vortices attained numerically are not necessarily quantized (i.e. $A_m(r \rightarrow \infty) = 4(m+1)$ is an approximate prediction, the effective values for $A_m(r \rightarrow \infty)$ being the ones in the Figure 2).

Now, it is important to clarify that, beyond the configurations we have presented above, there is also a particular first-order scenario that can not be predicted by any analytical construction, being not possible to approximate its solutions via $\alpha(r) \ll 1$.

In order to introduce these new solutions, we again solve the first-order equations (33) and (34) numerically according the conditions (10) and (32), from which we depict the resulting profiles in the figures 7, 8, 9, 10, 11 and 12 below. Here, we use $h = g = k = r_0 = 1$ and

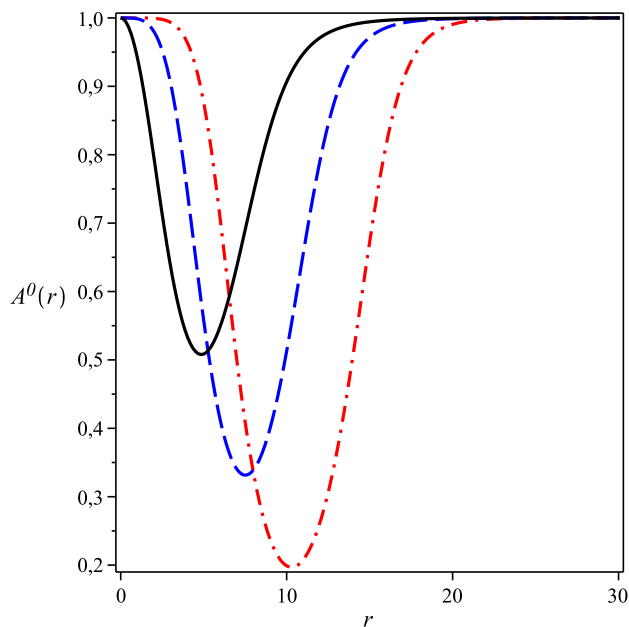


FIG. 11: Numerical solutions to $A^0(r)$. Conventions as in the Fig. 7. This field behaves in the same way as before.

$m = 1$ (solid black line), $m = 2$ (dashed blue line) and $m = 3$ (dash-dotted red line).

The new numerical solutions to $\alpha(r)$ are those depicted in the Figure 7, the resulting configurations behaving in the same way as before, i.e. being rings centered at the origin, their radii and amplitudes increasing as the vorticity m itself increases.

In the Figure 8, we show the profiles to the gauge function $A(r)$, the additional dotted orange line representing the solution for $m = 4$. Here, it is important to point out the existence of an interesting internal structure inherent to the new gauge profiles. Moreover, we emphasize that the new solutions do not obey $A(r \rightarrow \infty) \rightarrow 4(m+1)$, as expected.

The solutions to the magnetic field $B(r)$ and the energy density $\varepsilon_{bps}(r)$ appear in the figures 9 and 10, respectively, both ones standing for double rings centered at $r = 0$. In particular, the magnetic field satisfies $B(r = 0) = 0$ and $B(r \rightarrow \infty) \rightarrow 0$, the energy distribution vanishing at the origin for $m \neq 1$ only, with $\varepsilon_{bps}(r \rightarrow \infty) \rightarrow 0$ (i.e. the finite-energy requirement still holds).

Finally, the figures 11 and 12 show the numerical solutions to the electric potential $A^0(r)$ and the electric field $E(r)$, from which we see that these two fields behave in the same way as those depicted in the figures 5 and 6 (including the sign inversion inherent to the electric field), respectively, the electric one also possessing an internal structure, see the dotted orange line.

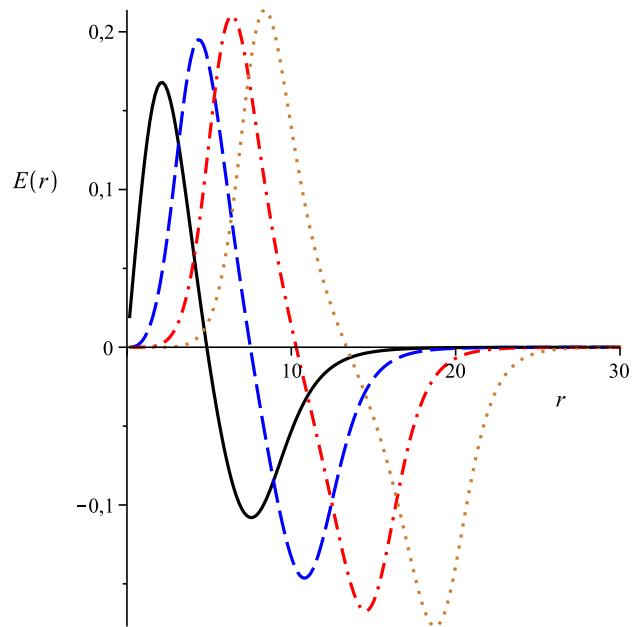


FIG. 12: Numerical solutions to $E(r)$. Conventions as in the Fig. 8. Note the internal structure inherent to the electric field.

IV. FINAL COMMENTS AND PERSPECTIVES

In this work, we have considered the nontopological first-order solitons inherent to a planar gauged $CP(2)$ scenario endowed by the Chern-Simons action, focusing our attention on those time-independent profiles possessing radial symmetry. We have proceeded the minimization of the corresponding energy (the starting-point being the energy-momentum tensor), from which we have established the corresponding first-order framework (a set of two coupled first-order equations and a well-defined lower bound for the total energy itself) inherent to the effective radially symmetric scenario. We have also pointed out the differences between the present construction and its counterpart introduced previously for the study of topological solitons [11].

In the sequel, we have used the first-order expressions we have found in order to calculate numerically legitimate first-order solutions by means of the finite-difference method. Here, despite the highly nonlinear expressions, we have identified a special kind of configurations that can be described by approximate analytical solutions in the regimen $\alpha(r) \ll 1$ for all r .

We have depicted the resulting numerical profiles, from which we have also commented on the main properties that they engender. In this sense, we have also noted an interesting inversion in the sign dictating the electric interaction and the existence of an internal structure inherent to the gauge function.

Interesting issues include the search for first-order solutions arising from a gauged $CP(2)$ theory endowed by the Maxwell's and the Chern-Simons terms simultaneously.

We are currently working on such idea, from which we expect positive results to be presented in a future contribution.

Acknowledgments

This work was supported by the CNPq, CAPES and FAPEMA (Brazilian agencies). In particular, RC

thanks the support from the grants CNPq/483863/2013-0, CNPq/306385/2015-5, FAPEMA/Universal-00782/15 and FAPEMA/Universal-01131/17, MLD acknowledges the full support from CAPES (postgraduate scholarship), and EH thanks the support from the grants CNPq/307545/2016-4 and CNPq/449855/2014-7.

-
- [1] N. Manton and P. Sutcliffe, *Topological Solitons* (Cambridge University Press, Cambridge, England, 2004).
- [2] E. Bogomol'nyi, *Sov. J. Nucl. Phys.* **24**, 449 (1976). M. Prasad and C. Sommerfield, *Phys. Rev. Lett.* **35**, 760 (1975).
- [3] H. B. Nielsen and P. Olesen, *Nucl. Phys. B* **61**, 45 (1973).
- [4] R. Jackiw and E. J. Weinberg, *Phys. Rev. Lett.* **64**, 2234 (1990). R. Jackiw, K. Lee and E. J. Weinberg, *Phys. Rev. D* **42**, 3488 (1990).
- [5] D. Bazeia, E. da Hora, C. dos Santos and R. Menezes, *Phys. Rev. D* **81**, 125014 (2010); *Eur. Phys. J. C* **71**, 1833 (2011). D. Bazeia, R. Casana, M. M. Ferreira Jr. and E. da Hora, *Europhys. Lett.* **109**, 21001 (2015). R. Casana, E. da Hora, D. Rubiera-Garcia and C. dos Santos, *Eur. Phys. J. C* **75**, 380 (2015). R. Casana, M. M. Ferreira Jr., E. da Hora and C. Miller, *Phys. Lett. B* **718**, 620 (2012). R. Casana, M. M. Ferreira Jr., E. da Hora and A. B. F. Neves, *Eur. Phys. J. C* **74**, 3064 (2014). R. Casana and G. Lazar, *Phys. Rev. D* **90**, 065007 (2014). R. Casana, C. F. Farias and M. M. Ferreira Jr., *Phys. Rev. D* **92**, 125024 (2015). R. Casana, C. F. Farias, M. M. Ferreira Jr. and G. Lazar, *Phys. Rev. D* **94**, 065036 (2016). L. Sourrouille, *Phys. Rev. D* **87**, 067701 (2013). R. Casana and L. Sourrouille, *Mod. Phys. Lett. A* **29**, 1450124 (2014).
- [6] C. Armendariz-Picon, T. Damour and V. Mukhanov, *Phys. Lett. B* **458**, 209 (1999). V. Mukhanov and A. Vikman, *J. Cosmol. Astropart. Phys.* **02**, 004 (2005). A. Sen, *J. High Energy Phys.* **07**, 065 (2002). C. Armendariz-Picon and E. A. Lim, *J. Cosmol. Astropart. Phys.* **08**, 007 (2005). J. Garriga and V. Mukhanov, *Phys. Lett. B* **458**, 219 (1999). R. J. Scherrer, *Phys. Rev. Lett.* **93**, 011301 (2004). A. D. Rendall, *Class. Quantum Grav.* **23**, 1557 (2006).
- [7] A. D'Adda, M. Luscher and P. D. Vecchia, *Nucl. Phys. B* **146**, 63 (1978). E. Witten, *Nucl. Phys. B* **149**, 285 (1979). A. M. Polyakov, *Phys. Lett. B* **59**, 79 (1975). M. Shifman and A. Yung, *Rev. Mod. Phys.* **79**, 1139 (2007).
- [8] A. Yu. Loginov, *Phys. Rev. D* **93**, 065009 (2016).
- [9] R. Casana, M. L. Dias and E. da Hora, *Phys. Lett. B* **768**, 254 (2017).
- [10] R. Casana, M. L. Dias and E. da Hora, *Phys. Rev. D* **96**, 076013 (2017).
- [11] V. Almeida, R. Casana and E. da Hora, *First-order vortices in a gauged CP(2) model with a Chern-Simons term*, arXiv:1709.05541 [hep-th]. Accepted for publication in the Physical Review D.